Taylor & Francis
Taylor & Francis Group

Science and Technology for the Built Environment

ISSN: 2374-4731 (Print) 2374-474X (Online) Journal homepage: http://www.tandfonline.com/loi/uhvc21

A field investigation of a solar-powered adsorption cooling system under Guangzhou's climate with various numbers of heat exchangers in the adsorbers

Long Qian Zhu, Chi Yan Tso, Wei He, Chi Li Wu & Christopher Y.H. Chao

To cite this article: Long Qian Zhu, Chi Yan Tso, Wei He, Chi Li Wu & Christopher Y.H. Chao (2017): A field investigation of a solar-powered adsorption cooling system under Guangzhou's climate with various numbers of heat exchangers in the adsorbers, Science and Technology for the Built Environment, DOI: 10.1080/23744731.2017.1296322

To link to this article: http://dx.doi.org/10.1080/23744731.2017.1296322

Science and Technology for the Built Environment (2017) **0**, 1–11
Copyright © 2017 ASHRAE.
ISSN: 2374-4731 print / 2374-474X online
DOI: 10.1080/23744731.2017.1296322

A field investigation of a solar-powered adsorption cooling system under Guangzhou's climate with various numbers of heat exchangers in the adsorbers

LONG QIAN ZHU[1], CHI YAN TSO[1,2,*], WEI HE[3], CHI LI WU[3], and CHRISTOPHER Y.H. CHAO[1]

[1]*Department of Mechanical and Aerospace Engineering, The Hong Kong University of Science and Technology, Hong Kong 999077, China*
[2]*HKUST Jockey Club Institute for Advanced Study, The Hong Kong University of Science and Technology, Hong Kong, China*
[3]*Buliding Energy Research Center, Guangzhou HKUST Fok Ying Tung Research Institute, Guangzhou, China*

In the current study, a solar-powered double-bed adsorption cooling system has been built and tested in the Guangzhou climate. The effect of the pre-heating process on the cooling performance of the adsorption cooling system powered by solar energy has been experimentally investigated. A specific cooling power of 52.2 W/kg and a coefficient of performance of 0.20 were achieved under a 2-h pre-heating process with operating conditions of 26°C cooling water inlet temperature, 16°C chilled water inlet temperature, 8 L/min hot water and cooling water flow rate, 2 L/min chilled water flow rate and 600 s adsorption/desorption phase time. The average specific cooling power and coefficient of performance were improved by 26.1% and 33.3%, respectively, as compared to the case without conducting the pre-heating process. In addition, the influence of dead volume on the specific cooling power and coefficient of performance of the adsorption cooling system has also been investigated. Using various numbers of heat exchangers in the adsorber achieved different values of adsorber dead volume. The results show that a higher specific cooling power value is obtained with a smaller dead volume. Finally, the cooling performance of the adsorption cooling system was also studied under various operating conditions and a maximum specific cooling power and coefficient of performance are 180.4 W/kg and 0.29, respectively.

Introduction

Climate changes such as global warming and the potential shortage of fossil fuel are leading to an increase in energy costs have motivated many industries and researchers to focus on high efficiency and renewable energy technologies. Buildings are one of the major energy consuming elements in cities. For example, the energy consumed in HVAC systems accounted for about 27% of the total consumption in 2013 in Hong Kong (EMSD 2013). Currently, vapor compression cooling systems are the most widely used refrigeration systems worldwide. However, operating a vapor compression cooling system not only consumes a lot of electricity, which is carbon unfriendly, but also has a negative effect on the ozone layer due to the use of refrigerants. Bearing these consequences in mind, attention is now focused on developing innovative, reliable, low pollution, and lower energy cost refrigeration systems. An adsorption cooling system (ACS) which is driven by low-grade heat sources, such as solar energy and waste heat, could satisfy these requirements (Nidal et al. 2010; Tso et al. 2014; Ullah et al. 2013; Wang 2001). Compared to vapor compression refrigeration systems, the ACS has two major advantages. First, a very small amount of electricity is required to drive the ACS, thus carbon dioxide emission, the electricity consumption and cost could be reduced (Anyanwu, 2004; Chan et al. 2012; Miyazaka et al. 2010). Second, pollution-free refrigerants, such as water and ammonia, are used in these systems. These refrigerants have zero ozone depletion potential compared to Freon (Anyanwu, 2004; Solmus et al. 2011; Tso and Chao 2012).

Researchers have been studying the technologies of ACSs since the energy crisis in the 1970s. However, ACSs have not received much attention compared to the absorption cooling systems since the efficiency of ACSs is not satisfactory and there are some technical problems that need to be solved (Loh et al. 2012; Thu et al. 2013; Tso et al. 2012; Wang et al. 2010), such as the bulky size of the systems, unsteady chilled water delivery, and the complicated operating sequence of the systems. In terms of application, the heat source becomes a key issue (Sapienza et al. 2011). Solar energy, waste heat or other low-grade heat sources can be used to drive the

---

Received August 17, 2016; accepted January 24, 2017
Long Qian Zhu, MSc, is a PhD Student. **Chi Yan Tso, DPhil,** is a Research Assistant Professor. **Wei He, BA,** is a Research Assistant. **Chi Li Wu, DPhil,** is a Research Associate. **Christopher Y.H. Chao, DPhil,** Member ASHRAE, is a Chair Professor.
*Corresponding author e-mail: mecytso@ust.hk
Color versions of one or more of the figures in the article can be found online at www.tandfonline.com/uhvc.

ACS. Solar energy is the most popular heat source for an ACS since it is easy to implement, environmentally friendly, and free of charge (Hassan et al. 2012). In 2011, Hassan and colleagues developed a realistic theoretical simulation model for a tubular solar-powered ACS. It was found that the solar average coefficient of performance (COP) and average specific cooling power (SCP) of the system are 0.211 and 2.326 W/kg for a whole day in summer in Calgary (Hassan et al. 2011). In 2014, Tso and colleagues developed another numerical model to predict the cooling performance of the ACS, and they found that the average COP and SCP of the ACS depend significantly on the solar collector temperature (or solar collector area). A double-glazed cover shows the best cooling performance, and the duration of the pre-heating process depends on the weather condition (solar intensity value; Tso et al. 2014). In 2015, Qasem and El-Shaarawi simulated the cooling performance of an adsorption ice maker under Dhahran's climate conditions. It was found that the best result of COP is obtained with a condensation temperature lower than 30°C. Besides, each square meter of solar collector can produce less than 3 kg of ice, and a COP of 0.3 was achieved in June (Qasem and El-Shaarawi 2015). Recently, Koronaki et al. (2016) developed a thermodynamic model to analyze a solar ACS in Mediterranean conditions in 2016. It was found that a flat plate collector coated with chromium selective coating is better than other collectors (e.g., a flat plate collector coated with black matte paint, a glazed PVT (hybrid photovoltaic/thermal collector) and an unglazed PVT). A maximum cooling capacity of 16 kW, a maximum COP of 0.51, and energy efficiency of 21.7% were achieved under the operating condition of a cooling water inlet temperature of 30°C, a chilled water inlet temperature of 14.8°C, a cooling water flow rate of 1.52 kg/s, a hot water flow rate of 1.28 kg/s, a chilled water flow rate of 0.71 kg/s, a cycle time of 900 s, and 47 kg silica gel adsorbents (Koronaki et al. 2016). Although the simulation took into account the variations of ambient environment temperature and solar radiation, the simulation results still cannot comprehensively represent a realistic performance of an ACS driven by solar energy. Therefore, experimental investigations of an ACS powered by solar energy must be carried out. In 2010, Nidal and colleagues experimentally and statistically optimized a solar-powered adsorption ice-maker. Under the optimum condition with an adsorbent mass of 50–60 kg, a tank volume of 0.2–0.23 m^3, a collector area of 3.5–4.5 m^2, and a tilt angle of the collector of 45° toward the south, a COP of 0.2, and a cooling production of 10 kg/day were achieved in Mediterranean area (Nidal et al. 2010). In 2013, Alam et al. designed and built a solar-powered ACS and tested its cooling performance under Tokyo's climate. They found that at least 15 solar thermal collectors (each of 2.415 m^2) are required to achieve a heat source temperature of 85°C in Tokyo. Under the operating condition with a hot/cooling water mass flow rate of 1.3 kg/s, a chilled water mass flow rate of 0.7 kg/s, a cooling water temperature of 30°C, a chilled water inlet temperature of 14°C, a cycle time of 1500 s, and 47 kg silica gel adsorbents, a maximum cooling capacity of 10 kW, and a maximum COP of 0.3 are achieved at noon with 15 solar collectors (Alam et al. 2013). In 2015, Ji et al. developed a solar adsorption ice-maker using a solar vacuum tube collector and investigated the cooling performance under Yunnan's climate conditions. A maximum cooling capacity of 8.4 kg/day and a maximum COP of 0.139 were achieved under the operating condition with cooling water of 18°C, an adsorption/desorption phase time of 1 h, hot water of 215 kg, and activated carbon adsorbent of 32 kg (Ji et al. 2015). Also, Ambarita and Kawai experimentally studied a solar-powered ACS using a flat-plate solar collector under Medan's climate conditions. The solar collector was sloped at an angle of 30° and 6 kg adsorbents were loaded. It was found that activated carbon shows a better COP than that of the activated alumina. A maximum solar COP of 0.085, a maximum hot generator temperature of 110.1°C, a minimum hot generator temperature of 24.2°C, a maximum evaporator temperature of 21.3°C, and a minimum evaporator temperature of 6.03°C were achieved with a maximum ambient temperature of 37.45°C, a minimum ambient temperature of 24.2°C and an average solar radiation of 17.42 MJ/m^2 (Ambarita and Kawai 2016). Although the ACSs powered by solar energy have been previously studied by others, the effect of a pre-heating process on the cooling performance of the ACSs has rarely been investigated experimentally. Most importantly, no one has experimentally reported the cooling performance of an ACS under Guangzhou's climate in May where the weather is usually cloudy, hot (ambient temperature of 20°C–32°C) and humid (relative humidity of 70%–80%).

The adsorber is the most essential component of ACSs. Because of the poor thermal conductivity of the adsorbent materials commonly used in ACSs, the heat and mass transfer abilities of the adsorbers that affect the performance of the system should be considered carefully during their design. Saha and co-authors developed a two-stage four-bed ACS, from which a cooling power of 3.2 kW and a COP of 0.36 were recorded (Saha et al. 2001). Alam and co-authors built another four-bed ACS, but helical copper tubes were utilized as the adsorbent beds. Also, a mass recovery cycle was conducted in their system. The results show that the COP and SCP were increased by 94.3% and 53.3%, respectively, compared to a conventional two-stage ACS (Alam et al. 2004). Wang and co-authors exploited an adsorbent bed with fluidized adsorbent. The average mass variation rate of R134a adsorbate was increased by 630% compared to a conventional adsorbent bed with solid adsorbents. However, the amount of fluidized adsorbent (activated carbon) utilized on the adsorbent bed could not be more than 3 kg because of the incomplete fluidization of the activated carbon in the adsorber/desorber (Wang et al. 2012). An adsorber with multi-adsorbent beds was proposed by Zhu et al. in 2013. Helical copper tubes covered by metal filters were employed in the adsorber, showing a 40% enhancement of adsorbent capacity when compared to a conventional design of the adsorber. The SCP and COP were recorded at 3.4 W/kg and 0.26, respectively (Zhu et al. 2013). Ammar and colleagues developed an ACS using a tubular adsorber and simulated the cooling performance under sub-Saharan climate conditions. The tubular adsorber consisted of eight thin and homogeneous metallic tubes. The external surface of tubes was coated with a selective black paint to absorb solar energy. The internal surface of tubes was perforated with small holes along the entire length to allow the adsorbate to pass through. The adsorbent was filled in between the external and internal surfaces. The simulation results show that the most optimized diameter of the adsorber tubes is 0.118 m and a total of 38.59 kg adsorbents can be filled in the tubes. At the same time, it was also found that the performance of the system using aluminum for the adsorber tubes wall is similar to that using copper. A maximum COP of 0.21 and a maximum cooling capacity of 14 MJ in 30 h were achieved under the operating condition with an adsorption temperature of 301.15 K, a condensation temperature of 313.15 K, and an evaporation temperature of 272.15 K (Ammar et al. 2015). Although many research groups have studied the effect of different adsorber designs on the cooling performance of the ACS, the influence of the dead volume (i.e., volume ratio of the empty part of the adsorber to that of the total adsorber volume) on the SCP and COP of ACS has rarely been investigated experimentally. The dead volume is one of the important issues to be considered for designing an adsorber since it may significantly affect the cooling performance of the ACS. Finally, various operating conditions are also investigated in this study since this affects the cooling performance of the ACS dramatically (Sapienza et al. 2011). Miyazaki et al. (2010) developed a novel dual-evaporator adsorption chiller with three adsorbent beds, and they tested the effect of operating temperatures and cycle time on the SCP and COP. It was found that higher the chilled water inlet temperature, the higher the SCP and COP. Tso et al. (2012) simulated and experimentally investigated (Tso et al. 2015) the effect of adsorption/desorption phase time, hot water inlet temperature, cooling water inlet temperature, and chilled water inlet temperature on the SCP and COP. The results indicate that these parameters have a great influence on the cooling performance of the ACS such that an optimization study must be carried out in order to achieve the maximum SCP and COP of an ACS.

Although many researchers have studied the ACSs, the effect of the pre-heating process on the cooling performance has rarely been experimentally investigated, especially under Guangzhou's climate condition. Besides, the effect of the dead volume on the cooling performance of the ACSs has also rarely been experimentally investigated. Overall, this study aims at building a double-bed ACS using vehicle radiator (heat exchanger) as the adsorbent bed to:

1. Investigate the real-time cooling performance of the system driven by solar energy under Guangzhou' climate. The SCP and COP are the major figures of merit;
2. Study the influence of the pre-heating process on the cooling performance of the system. The pre-heating process is required to ensure that the solar collector temperature is high enough to activate the operation of the ACS. Ideally, this pre-heating process should be as short as possible so that the solar-powered ACS could be operated for a longer period during the day. In this study, for simplicity, the influence of the pre-heating process and without conducting the pre-heating process on the SCP and COP of the ACS is investigated;
3. Investigate the effect of the adsorber dead volume on the SCP and COP of the ACS. Four adsorbers with various numbers of heat exchangers placed inside the adsober are built, implying that four different values of dead volume in adsorber are studied;
4. Optimize the operating conditions (i.e., desorption temperature, adsorption/desorption phase time, mass recovery time, and heat recovery time).

Silica gel—water is used as the adsorbent—adsorbate working pair in this study. It should be pointed out that solar energy, which is unstable because of different weather conditions, is utilized to power the ACS for the first two objectives as previously mentioned, while electrical heaters are used to drive the ACS for studying the last two objectives since a stable heat source is required for investigating the influence of dead volume on the cooling performance of the ACS as well as the system optimization. A stable and controllable hot water inlet temperature can be provided to the ACS with electrical heaters, so that the cooling performances of the ACS utilizing four adsorbers with various numbers of heat exchangers can be compared with each other under the same operating condition, and the operating conditions can be optimized with a control variate method.

Description of the ACS

Working principle of the ACS

ACS can be compared to conventional vapor compression cooling systems, with the compressor being replaced by a thermally driven adsorber. Solar energy or waste heat can be used as a heat source for desorption purposes, making the ACS more attractive in terms of saving electricity. Also, the adsorption/desorption cycles can be operational without moving parts other than magnetic valves, thus leading to low vibration, mechanical simplicity, high reliability, and a very long life time.

The working principle of an ACS is that a large amount of adsorbent packing in an adsorbent bed adsorbs the adsorbate from an evacuated container (evaporator) so that the adsorbate in the evaporator continuously evaporates at low pressure to cool the process air. Cooling water must be supplied to the adsorbers in order to remove the adsorption heat generated by the adsorbents. After a couple of minutes, the adsorbent will be almost saturated with adsorbate, which means there is no more space for the adsorbent to adsorb the adsorbate. As a result, the adsorbent has to be heated for performing the desorption process. As the pressure of the desorber is higher than that of the condenser during the desorption process, the adsorbate will flow automatically from the desorber to the condenser, condense in the condenser, and then return to the evaporator due to the gravitational effect, as well as the pressure difference between the condenser and evaporator. Cooling water has also to be supplied to the condenser at the same time in order to remove the condensation heat. The thermodynamic cycle for both the adsorption and desorption process is then completed. As an energy efficient solution, the hot water can be heated by solar energy and/or low grade waste heat. Two adsorbers work alternately in order to produce the cooling effect continuously since the

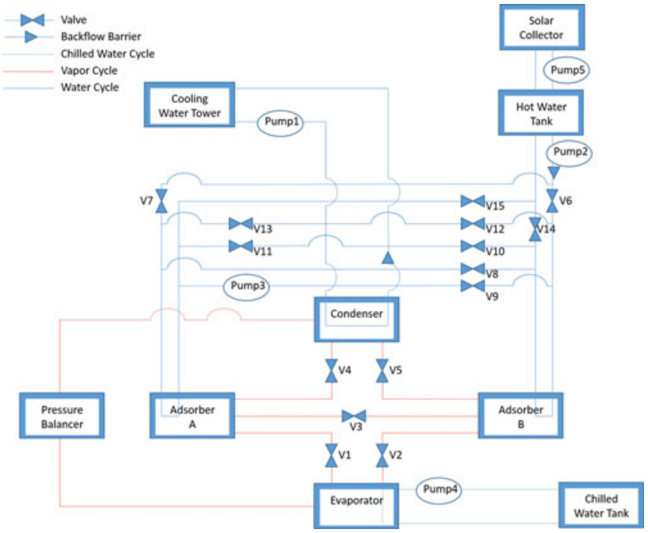

Fig. 1. A schematic design of the ACS powered by solar energy.

cooling effect is only produced during the adsorption phase. A schematic design of the ACS is shown in Figure 1.

Operating sequence

Basically, the operating cycle of a double-bed ACS consists of two major phases. In phase I, adsorber A is in adsorption phase while adsorber B is in desorption phase. The adsorbate (water vapor in the current study) evaporates in the evaporator at the evaporation temperature, T_{eva}, and the water vapor flows to adsorber A. The water vapor is adsorbed by the adsorbent (silica gel in this study) in adsorber A and cooling water passing through the adsorber removes the heat generated due to the adsorption phase. The desorber (adsorber B) on the other hand is heated to the desorption temperature, T_{des} by hot water passing through the adsorber from the hot water tank. The water vapor is desorbed from the adsorbents in adsorber B and flows to the condenser. Cooling water passing through the condenser removes the heat generated due to the condensation of water vapor. The condensed adsorbate flows back to the evaporator via the pressure controller which is connected between the condenser and evaporator. Phase II is similar to Phase I, but adsorber A is heated to desorb while adsorber B is cooled to adsorb. Therefore, the basic operating sequence of the ACS can be described as "Phase I → Phase II → Phase I → Phase II → …"

After conducting Phase I, a mass recovery cycle, called Phase I-M, is always to be conducted for further enhancing the cooling performance of the system. In Phase I-M, adsorber A and adsorber B are connected, while the cooling water from the cooling water tower continues to be supplied to adsorber A and hot water continues to be supplied to adsorber B. By connecting the two adsorbers together, the adsorbate flows from a higher pressure adsorber (adsorber B) to a lower one (adsorber A) automatically. Adsorber A is pressurized and adsorber B is depressurized, causing further desorption of the adsorbent in adsorber B and further adsorption in adsorber A. Therefore, it can be easily understood that mass recovery can further dry the heated adsorber after desorption and reduce the internal pressure. Similarly, another mass recovery cycle, called Phase II-M, is operated after Phase II. Hot water continues to be supplied to adsorber A and cooling water continues to be supplied to adsorber B, and no adsorbers are connected with the evaporator or condenser in Phase II-M. (Akahira et al. 2004; Khan et al. 2007; Qu et al. 2001).

The heat recovery cycle, which is called Phase H in the current study, is conducted after the mass recovery cycle. After adsorption phase, the temperature of the corresponding adsober is low, while the other adsorber is heated after the desorption phase. The heat transfer fluid (water in this study) flows through two adsorbers to transfer the heat from the heated adsorber to the cooled adsorber. By circulating the heat transfer fluid between two adsorbers, the energy efficiency can be increased significantly. In the heat recovery cycle, about 30% of thermal energy of the total necessary heat input of the desorption phase can be recovered (Chan et al. 2015; Li et al. 2009; Qu et al. 2001). A complete operating sequence of the ACS investigated in this study is expressed as: "Phase I → Phase I-M → Phase H → Phase II → Phase II-M → Phase H → Phase I → …"

Test unit

Figure 2 shows the front view and side view of an ACS built in the laboratory in Nansha, Guangzhou, while Figure 3 shows a chilled water tank, cooling water tower, and three solar thermal collectors. The chilled water tank is located indoors, delivering stable chilled water to the ACS. The cooling water tower, located outside, is used to provide cooling water to two adsorbers as well as the condenser of the ACS. The solar thermal collectors are installed on the rooftop of a building to offer heat sources to the ACS such that the feasibility of an ACS powered by solar energy can be realized. Three flat plate solar thermal collectors with a total surface area of 6 m^2 are employed and they are connected in parallel.

The dimensions of the adsorber designed in this study are 600 mm (height) × 390 mm (length) × 390 mm (width). Adsorbent beds in the adsorber are regarded as heat exchangers. Vehicle radiators are one of the choices for use as the adsorbent bed because of their lower cost and simplified assembly processes. Silica-gel adsorbents are put in between the fins of the radiator. The radiators have to be covered by stainless steel metal meshes with a nominal pore size of 250 microns to prevent the adsorbents leaking out from the radiators. Metal frames are used to hold the stainless-steel metal meshes. Figure 4 shows photos of a raw heat exchanger (vehicle radiator), and the heat exchanger covered by a stainless-steel metal mesh and metal frame. Four adsorbers with different dead volume values are built. As previously mentioned, the dead volume in the adsorber is defined as the volume ratio of the empty part of the adsorber to that of the total adsorber volume, and it is calculated by Equation 1:

$$D = \frac{V_{ad} - V_{adso}}{V_{ad}} \times 100\%, \tag{1}$$

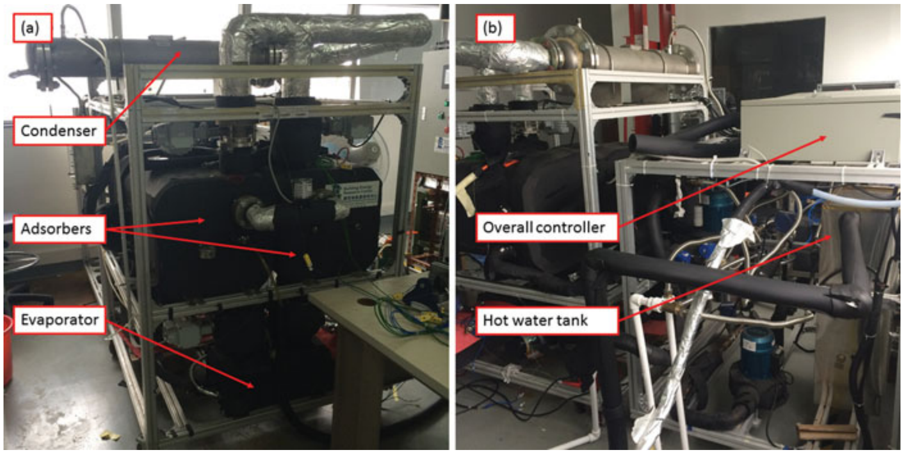

Fig. 2. The a. front view; and b. side view of the ACS prototype.

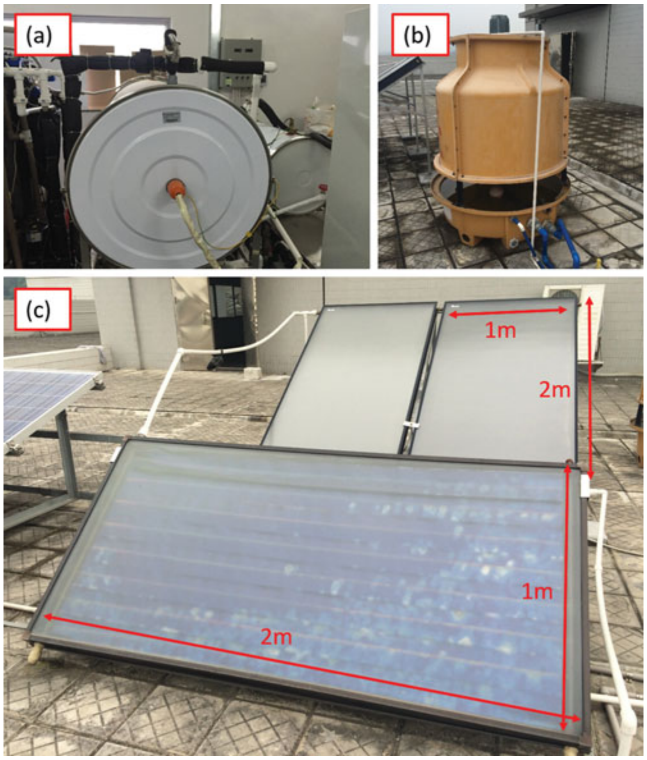

Fig. 3. Photos of a. chilled water tank; b. cooling water tower; and c. several solar thermal collectors.

where D represents the dead volume of the adsorber [%], V_{ad} refers to the volume of the adsorber [m^3], while V_{adso} denotes the volume of the adsorbent bed [m^3]. In other words, $V_{ad} - V_{adso}$ refers to the empty volume in the adsorber [m^3]. Table 1 shows the specification of the four different adsorbers tested in the current study. It should be noted that the heat exchangers in the adsorbers are connected in series. Figure 5 shows a photo of an adsorber with seven adsorbent beds (heat exchangers). The size of the heat exchanger (i.e., vehicle radiator) covered with metal mesh and frame is 410 mm (length) × 365 mm (width) × 30 mm (thickness). According to the specification provided by the supplier, the particle size of the adsorbent ranges from 0.5 to 1 mm, thus 1 kg of silica-gel adsorbents is used to fill each heat exchanger. As

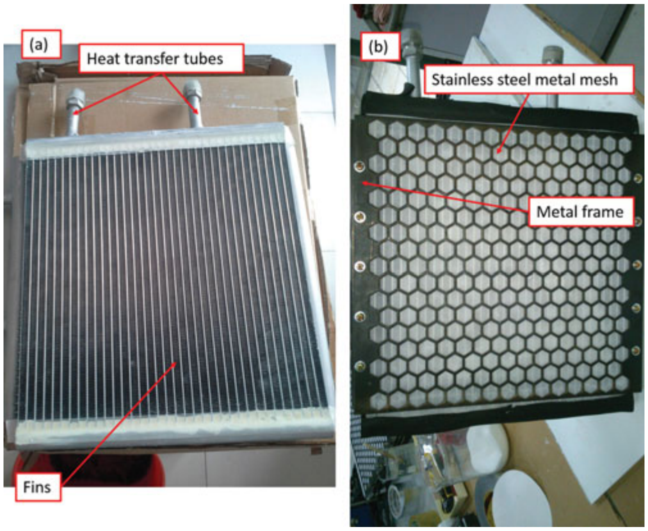

Fig. 4. Photos of a. heat exchanger (vehicle radiator); and b. the heat exchanger covered by stainless steel metal mesh and metal frame.

Table 1. Specification of the four different adsorbers tested in this study (it should be noted that each heat exchanger can be filled in 1 kg silica-gel adsorbent).

Type	Number of heat exchangers in one adsorber	Dead volume, %	Weight of silica-gel adsorbent in one adsorber, kg
1	5	75.4	5
2	6	70.5	6
3	7	65.6	7
4	8	60.6	8

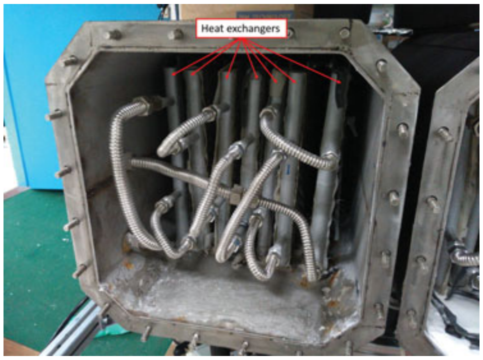

Fig. 5. A photo of an adsorber with seven adsorbent beds (heat exchangers).

previously mentioned, for the first two objectives of this study, the ACS is powered by solar power, meanwhile for the remaining objectives of this study, a stable heat source (electrical heaters) is required to provide a steady desorption temperature to the ACS. Two electrical immersion heaters with 2 and 1 kW power are employed.

K type thermocouples are utilized in different locations of the system to monitor and record the temperature of the hot water, cooling water and chilled water. All the thermocouples are recorded by data acquisition (DAQ) devices from National Instruments. The thermocouple signals are recorded by the SCXI-1102 32-Channel Thermocouple/Voltage Input Module with a SCXI-1324 terminal block equipped with the SCXI-1001 chassis connected to a computer. NI LabVIEW (version 8.6) software is used to build a virtual DAQ program. Data is recorded every 3 s and stored on the computer's hard disk. The solar intensity is measured by a data logging solar intensity meter, e-model number TES-1333R. The solar intensity meter is located near the solar thermal collectors, and its surface is parallel to that of the solar thermal collectors. The ATmega128 micro-controller unit (MCU) module and a relay module are used to realize the control of the valve system, and this is implemented through software programming.

System evaluation

Equation 2 is used to calculate the solar COP of the ACS:

$$COP_{so} = \frac{\int_0^{t_{cycle}} \left(\frac{Q_{chill}}{Q_{des,so}}\right) dt}{\int_0^{t_{cycle}} dt}, \tag{2}$$

where Q_{chill} represents the cooling output power [W], $Q_{des,so}$ represents the thermal input power from the solar thermal collectors [W] and t_{cycle} represents the time required for the ACS to finish a complete cycle(s). The COP of the system driven by electrical heaters is calculated by Equation 3:

$$COP_{he} = \frac{\int_0^{t_{cycle}} \left(\frac{Q_{chill}}{Q_{des,he}}\right) dt}{\int_0^{t_{cycle}} dt}, \tag{3}$$

where $Q_{des,he}$ represents the thermal input power from the electrical heaters [W]. The cooling output power is calculated by Equation 4:

$$Q_{chill} = \dot{m}_{chill} c_{p,water} (T_{chill,in} - T_{chill,out}), \tag{4}$$

where $\dot{m}_{chill}$ refers to the mass flow rates of the chilled water [kg/min], $c_{p,water}$ denotes the specific heat capacity of the water [J/(kgK)], $T_{chill,in}$ and $T_{chill,out}$ represent the inlet and outlet temperatures of the chilled water (°C), respectively. The thermal input power from the solar collectors and electric heaters are calculated by Equation 5 and 6, respectively:

$$Q_{des,so} = \dot{m}_{hot} c_{p,water} (T_{so,in} - T_{so,out}), \tag{5}$$

where $\dot{m}_{hot}$ refers to the mass flow rates of the hot water [kg/min], $T_{so,in}$ and $T_{so,out}$ represent the inlet and outlet water temperature of the solar thermal collectors (°C), respectively.

$$Q_{des,he} = \dot{m}_{hot} c_{p,water} (T_{hot,in} - T_{hot,out}). \tag{6}$$

It should be noted that as the thermal input power is obtained from the temperature difference between the inlet and outlet of the hot water tank, heat loss to the ambient environment is included in the calculation. The energy loss is mainly from the adsorbers, hot water tank, and piping system through which the heat transfer fluid (water) circulates. Finally, Equation 7 is used to calculate the SCP of the ACS:

$$SCP = \frac{Q_{chill}}{W}, \tag{7}$$

where W represents the weight of the adsorbents used in an adsorber [kg].

Results and discussions

The influence of pre-heating process on the average SCP and COP of the ACS powered by solar energy

To begin, seven heat exchangers were utilized to form an adsorber for the real-time cooling performance testing. In other words, the amount of the silica-gel adsorbents utilized in this case was 7 kg in each adsorber. Solar energy was used to drive the ACS. The tests, on May 5th and 6th of 2016, started at 8:00 am and continued until 4:00 pm in Nansha, Guangzhou, China. The ambient temperature on May 5th varied from 24°C to 31°C, while the ambient temperature on May 6th varied from 25°C to 31°C. The ambient air temperatures on these two days were very close to each other. Figures 6 and 7 show the temperature profile of the heat transfer fluid (water) at different locations in the ACS, together with the solar intensity profile on May 5th and 6th of 2016, respectively. It should be noted that the test on May 5th was the case without conducting the pre-heating process at 8:00 am, while the test on May 6th is the case which did conduct

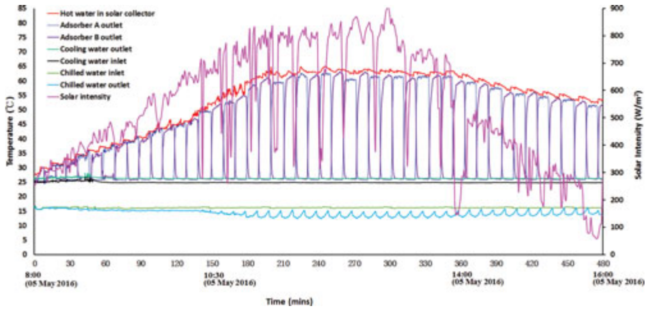

Fig. 6. Temperature profiles of the heat transfer fluid at different locations of the ACS, together with solar intensity profile on May 5, 2016 in Guangzhou (no pre-heating process at 8:00 am).

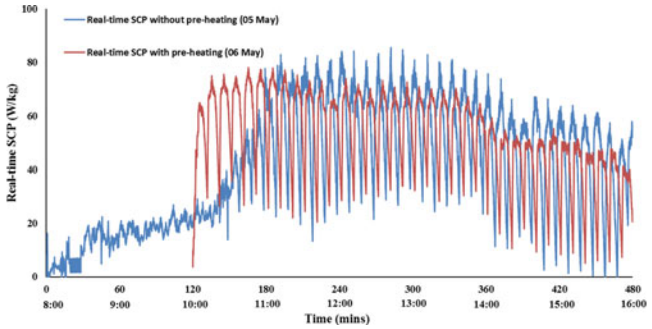

Fig. 8. The effect of the pre-heating process on real-time SCP.

the pre-heating process at 8:00 am (2 h pre-heating duration). In Figure 6, it can be seen that the hot water temperature in the solar thermal collector was about 25°C at 8:00 am on May 5th, and it increased to about 64°C at 12:00 pm, after that it stayed almost constant until 2:00 pm. The hot water temperature in the solar thermal collector started to decrease slowly after 2:00 pm due to the reduction in solar intensity. The chilled water outlet temperature was very close to the chilled water inlet temperature when the hot water temperature was below 50°C, implying that the minimum desorption temperature for this ACS is about 50°C (Saha et al. 2006). In Figure 7, it can be seen that the hot water temperature can increase to 64°C after conducting the 2-h pre-heating duration, and the temperature then slightly decreased to 61°C since hot water is supplied to the ACS to perform the desorption process at 10:00 am. This temperature reduction depends on the volume of the hot water tank (0.048 m^3 in this study). A larger hot water tank leads to a smaller temperature reduction. Similar to the temperature profile from May 5th, the hot water temperature shown on the May 6th was maintained for about 3 h (10:00 am–1:00 pm), and then it decreased slowly due to the decrease in solar intensity. It should be emphasized that the hot water temperature in the solar thermal collector reached the peak value in a shorter duration when the pre-heating process was performed even with a weaker solar intensity profile on May 6, 2016. The chilled water outlet temperature was always below the inlet temperature when the system included the pre-heating process. However, without conducting the pre-heating process, the system had almost no cooling effect, if and only if, the hot water temperature was higher than 50°C. The largest temperature difference between the chilled water inlet and outlet was 3.5°C between 12:00 pm to 2:00 pm (May 5, 2016) since the hot water temperature in the solar thermal collector was higher than 60°C which provided the energy to desorb the water vapor out from the silica gel adsorbent. On the other hand, although the largest temperature difference between the chilled water inlet and outlet on May 6, 2016 was still about 3.5°C, it reached this at an earlier time (at about 10:30 am on May 6, 2016) due to the implementation of the pre-heating process. In Figure 8, it can be seen that the pre-heating process can significantly improve the starting cooling performance. The average SCP from 8:00 am to 9:00 am on May 5th (without the pre-heating process) was only 9.64 W/kg, while the average SCP from 10:00 am to 11:00 am on May 6th (with the pre-heating process) was 59.87 W/kg, which was an increase of 521.06%. It should also be noted that without the pre-heating process (May 5th), the ACS almost had no cooling effect during the first 3 h (from 8:00 am to 11:00 am), but after 11:00 am, the SCP was slightly higher than that on May 6th since the solar intensity on May 5th was higher, leading to a higher desorption temperature. Under the operating conditions of a 25°C cooling water inlet temperature, 16°C chilled water inlet temperature, 8 L/min hot water and cooling water flow rate, 2 L/min chilled water flow rate, 600 s adsorption/desorption phase time, an average SCP of 41.4 W/kg and an average COP of 0.15 were achieved on May 5, 2016, while an average SCP and COP of 52.2 W/kg and 0.2 were obtained on May 6, 2016 (with 2 h pre-heating duration). Table 2 shows the average SCP and COP of the

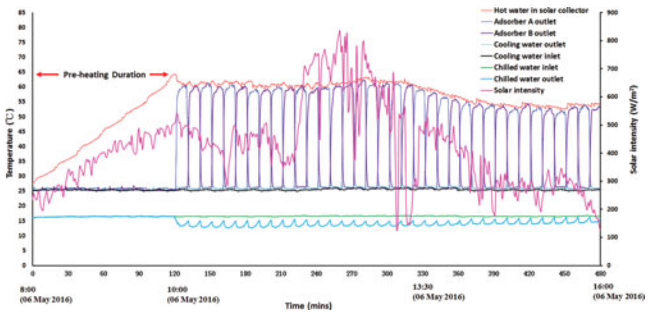

Fig. 7. Temperature profiles of the heat transfer fluid at different locations of the ACS, together with solar intensity profile on May 6, 2016 in Guangzhou (2 hours pre-heating process at 8:00 am).

Table 2. Cooling performance of the ACS powered by solar energy with and without conducting the pre-heating process.

Case	Average SCP, W/kg	ΔSCP, %	Average COP	ΔCOP, %
Without pre-heating process	41.4	N.A.	0.15	N.A.
With pre-heating process	52.2	26.1	0.20	33.3

ACS powered by solar energy with and without the pre-heating process. It can be seen that the average SCP increased by 26.1% with the pre-heating process compared to that without conducting pre-heating process even under the weaker solar intensity condition on May 6, 2016. In other words, the average SCP improvement could be even larger if it was under the same solar intensity profile. Regarding the average COP, it increased by 33.3% with the pre-heating process compared to that without conducting a pre-heating process. Without conducting the pre-heating process on May 5th, the cooling effect was very limited because of the low hot water temperature during the first 3 h (from 8:00 am to 11:00 am). During this period, the COP was also very low, at about 0.1. When the hot water temperature was higher than 50°C (i.e., after 11:00 am), the COP increased to about 0.18, and the average COP on May 5th was recorded at 0.15. With conducting the pre-heating process, the COP could reach about 0.2 quickly at the beginning because of a higher desorption temperature (60°C), and the average COP on May 6th was recorded at 0.2, showing a 33.3% improvement. Overall, both the average SCP and average COP were increased after conducting the pre-heating process since a much larger amount of thermal energy stored in the solar collectors led to a much higher hot water temperature at the beginning of the experiment. Almost all of the energy absorbed by the solar collectors was used to heat up the water inside the solar collectors which led to a rapid increase of the hot water temperature. However, without conducting the pre-heating process, the hot water temperature inside the solar collectors was low (slightly higher than the ambient temperature) at the beginning of the experiment.

The effect of dead volume on the SCP and COP of the ACS powered by electrical heaters

As shown in Table 1, a total of four different adsorbers were developed. The difference among those four different adsorbers was the numbers of heat exchangers utilized inside the adsorber. For example, type one adsorber consisted of five heat exchangers. As each heat exchanger can carry out 1 kg silica-gel adsorbent, the total amount of silica-gel adsorbent used to fill type one adsorber was 5 kg. It should also be pointed out that the dead volume decreased by about 5% when one more heat exchanger was inserted into the adsorber.

The effect of the four different adsorbers on the SCP and COP were investigated under the same operating conditions of 90°C hot water inlet temperature, 25°C cooling water inlet temperature, 16°C chilled water inlet temperature, 8 L/min hot water and cooling water flow rate, 2 L/min chilled water flow rate, and 600 s adsorption/desorption phase time. It should be emphasized that a steady heat source (electrical heater) is required to provide the heat input to the ACS for performing the desorption cycle such that the influence of dead volume on the cooling performance of the ACS can be well-studied.

In Figure 9, the results show that the SCP increased from 136.3 to 150.2 W/kg with the decrease of the dead volume from 75.4% to 60.6%, indicating a 10.2% improvement. Regarding the COP, it increased from 0.25 to 0.27, but this enhancement is not significant. Overall, a smaller value of dead volume leads to a better cooling performance of the ACS. This may be because more water vapor is stored in the adsorber when the dead volume is larger, leading to a slower vapor diffusion process and more energy being wasted, in addition to a longer time being required for the water vapor to flow into the condenser during the desorption phase when the dead volume is larger. Therefore, an adsorber design with the smallest dead volume is always preferable since it can provide the best SCP result.

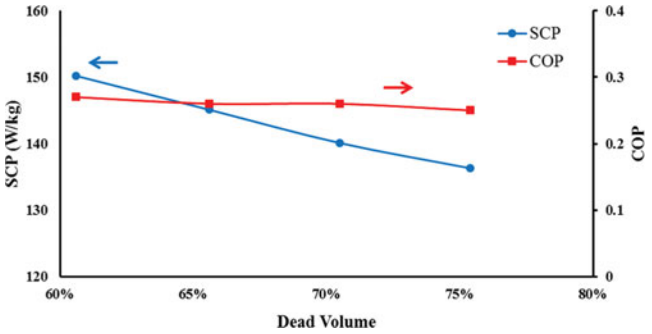

Fig. 9. The effect of the adsorber dead volume on the SCP and COP of the ACS powered by electric heaters.

Optimization of the operating conditions

In this section, various operating conditions of the ACS are investigated. As the best SCP result was obtained under the smallest adsorber dead volume, eight heat exchangers (vehicle radiators) connected in series are put in the adsorber to optimize the operating condition of the ACS. The standard operating conditions for the ACS are shown in Table 3, and also for various conditions as listed in Table 4. Figure 10a shows the effect of the hot water inlet temperature (desorption temperature) on the SCP and COP. All system parameters remained the same as shown in Table 3, except for the

Table 3. Standard operating condition for the ACS powered by electrical heaters.

Parameters	Values	Units
Hot water inlet temperature (desorption temperature), T_{hot}	90	°C
Cooling water inlet temperature, T_{cool}	25	°C
Chilled water inlet temperature, T_{chill}	16	°C
Hot water flow rate, $\dot{m}_{hot}$	8	L/min
Cooling water flow rate, $\dot{m}_{cool}$	8	L/min
Chilled water flow rate, $\dot{m}_{chill}$	2	L/min
Adsorption/desorption phase time, $t_{ads,des}$	600	s
Mass recovery time, t_{mr}	65	s
Heat recovery time, t_{hr}	55	s

Table 4. Varied operating conditions for the ACS powered by electrical heaters.

Parameters	Values	Units
Hot water inlet temperature (desorption temperature), T_{hot}	55, 65, 75, 85	°C
Adsorption/desorption phase time, $t_{ads,des}$	480, 540, 660, 720	s
Mass recovery time, t_{mr}	55, 75, 85, 95	s
Heat recovery time, t_{hr}	45, 50, 60, 65	s

desorption temperature which is considered as a varied operating parameter. The desorption temperature had a significant influence on the SCP since the SCP improved by 197.1% at the temperature of 90°C compared to that at 55°C. More water vapor was desorbed out from the adsorber with a higher temperature, thus the adsorbents could adsorb more water vapor in the next adsorption phase so that the SCP could be enhanced. In addition, it was also found that the SCP values of the ACS were close to each other (≈11% difference) no matter whether the system was powered by solar energy or electrical heaters. In Figure 7, the average SCP is found to be 52.2 W/kg with an average desorption temperature of 60°C, while the SCP is estimated at about 58 W/kg with a stable desorption temperature of 60°C (from Figure 10a). However, it should be noted that the former refers to the average SCP, and is powered by solar energy, meanwhile the latter is powered by a stable electrical heater. Therefore, a difference must exist between these two SCP values. In Figure 10b, it should be pointed out that the adsorption/desorption phase time was controlled by an automatic control system operating all valves and pumps, instead of by changing the hot water mass flow rate, etc. From Figure 10b, it is shown that 660 s is the best adsorption/desorption phase time for this ACS. This is because for shorter adsorption/desorption phase times, the desorption process is incomplete, leading to diminishing the adsorption capacity of the adsorbents. As a result, the SCP was low at a shorter phase time. For longer phase times, the SCP decreased due to the rapid diminution of adsorption capacity of the adsorbents during the last few minutes. Theoretically, with a longer adsorption/desorption phase time, the consumption of driving heat would be reduced at a faster rate than the reduction of the produced cooling power in the chilled water. This would lead to a favorable effect on the COP. In reality, the COP decreased after a long adsorption/desorption phase time because of the heat loss from the tubes, adsorbers, and hot water tank. In short, 660 s is the optimized adsorption/desorption phase time for this particular ACS. Figure 10c shows the effect of mass recovery time on the SCP and COP. The peak of SCP occurred when the mass recovery time was 85 s, while the peak of COP occurred when the mass recovery time was around 75 s. In the mass recovery cycle, water vapor transferred from the high pressure desorber to the low pressure adsorber, which allowed the desorber to decrease its pressure quickly for the next desorption phase and allowed the adsorber to increase its pressure

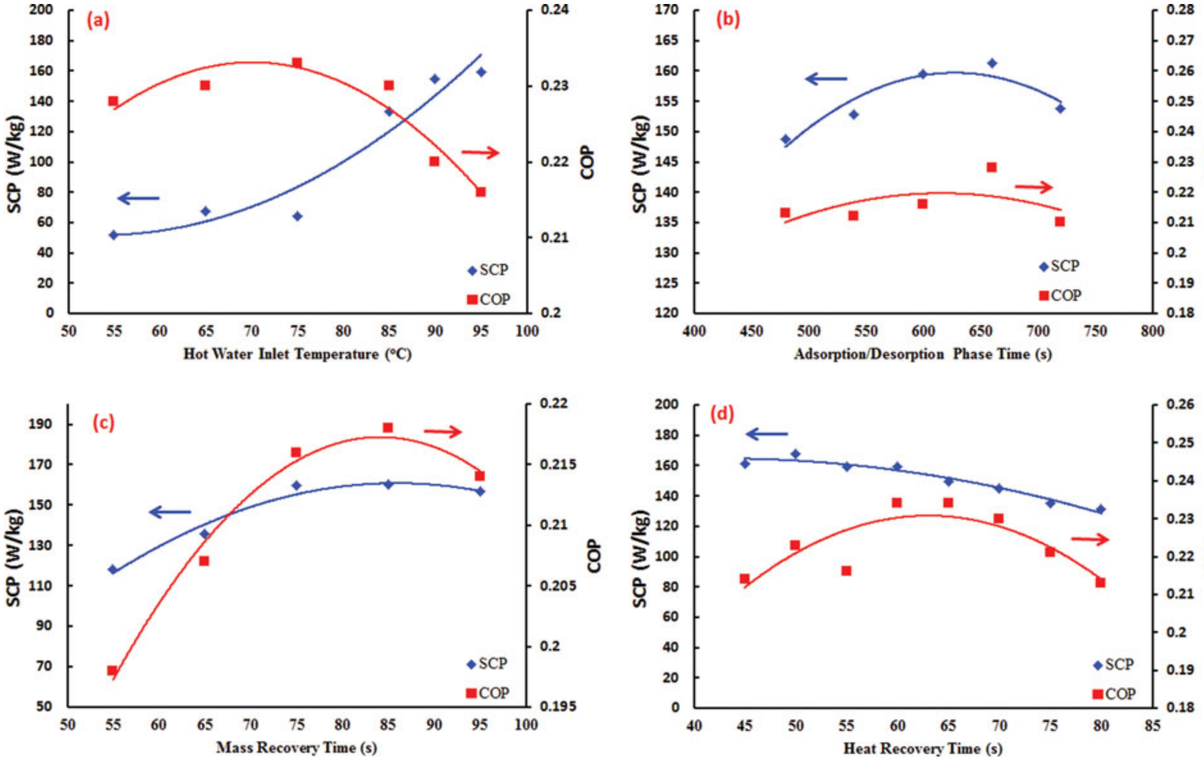

Fig. 10. The effect of a. hot water inlet temperature; b. adsorption/desorption phase time; mass recovery time; c. heat recovery time; and d. on the SCP and COP of the ACS.

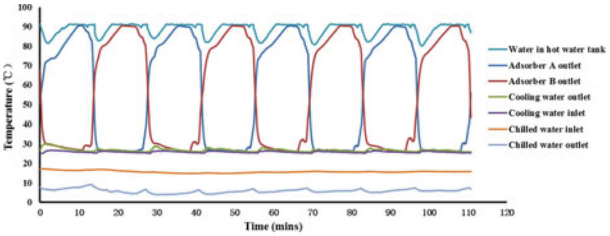

Fig. 11. Temperature profiles of the heat transfer fluid at different locations of the ACS with the optimized operating condition.

quickly for the next adsorption phase. At the same time, the desorber could be further dried during mass recovery. In this case, the SCP was enhanced. It should be noted that no cooling effect was produced during the mass recovery, implying the need for a shorter mass recovery time. However, a shorter mass recovery time might not give a better cooling performance due to an incomplete mass recovery process. Therefore, 85 s is selected as the optimized mass recovery time in this study since the SCP is more important than the COP. The SCP relates to how large the ACS is and the cooling power of the ACS.

In addition to the mass recovery cycle, the heat recovery cycle can also improve the system performance. The improvement is shown in Figure 10d. The SCP increased with the duration of heat recovery, and decreased when the duration was longer than 50 s. This is because the heat recovery was completed at about 50 s. A lengthy heat recovery process had no further benefit but unnecessarily increased the cycle time, reducing the SCP. The maximum SCP was 167.8 W/kg at 50 s. Although the COP increased with the duration of the heat recovery cycle, this enhancement was actually very small, and thus it can be ignored (i.e., from 0.21 to 0.23). Under the optimized operating condition of 90°C hot water temperature, 25°C cooling water inlet temperature, 16°C chilled water inlet temperature, 8 L/min hot water and cooling water flow rate, 2 L/min chilled water flow rate, 660 s adsorption/desorption phase time, 85 s mass recovery time, and 50 s heat recovery time, the ACS had a SCP of 180.4 W/kg and a COP of 0.29. The experimental temperature profiles of the heat transfer fluid (water) at different locations of the ACS under this optimized operating condition are shown in Figure 11.

Summary

In the current study, a double-bed silica gel—water ACS powered by solar energy was designed and built. The major outcomes of this study are that the ACS can be powered by solar energy under Guangzhou's hot and humid climate, in which the average SCP and COP can be achieved at 52.2 W/kg and 0.2, respectively, showing a great potential for practical application. Further, it was found that the SCP of the ACS which implemented the pre-heating process was improved by 26.1% compared to that without conducting the pre-heating process, proving that conducting a pre-heating process can help to enhance the cooling performance. In addition, the effect of dead volume on the cooling performance of the ACS was also investigated and it is found that the SCP was improved by reducing the dead volume. With the decrease of the dead volume from 75.4% to 60.6%, the SCP increased to 150.2 W/kg, showing a 10.2% improvement. Finally, the operating parameters were optimized. A SCP of 180.4 W/kg and a COP of 0.29 were achieved under the optimized operating condition of 90°C hot water temperature, 25°C cooling water inlet temperature, 16°C chilled water inlet temperature, 8 L/min hot water and cooling water flow rate, 2 L/min chilled water flow rate, 660 s adsorption/desorption phase time, 85 s mass recovery time, and 50 s heat recovery time. From these results, it is confirmed that the performance of the ACS can be improved by better adsorber design and operation optimization. In future works, the effect of the duration of pre-heating process can be investigated, the area of the solar thermal collector must be optimized, and also a solar tracker system will be utilized. Moreover, adaptive control with fuzzy logic will be studied to operate the ACS to better cope with real cooling load variations. With more future developments, the ACS can be installed in buildings to reduce the energy consumption for cooling production toward net-zero energy buildings.

Nomenclature

$C_{p,water}$ = specific heat capacity of water, J/(kgK)
COP = coefficient of performance
D = dead volume, %
$\dot{m}$ = mass flow rate, kg/min
P = pressure, Pa
Q = power, W
SCP = specific cooling power, W/kg
T = temperature, °C
t = time, s
V = volume, m^3
W = mass, kg

Subscripts

ads = adsorption
chill = chilled water
cool = cooling water
cycle = cycle
des = desorption
eva = evaporation
he = heater
hot = hot water
hr = heat recovery
in = inlet
mr = mass recovery
out = outlet
so = solar

Funding

Funding sources for this research are provided by the International Science and Technology Cooperation Program of the Science and Technology Program of Guangzhou, China via Grant No. 2013J4500064, Science and Technology Planning Project of Guangdong Province, China via Grant No. 2013B050900020 and Grant No. 2014B090903007, and the Hong Kong Research Grant Council via General Research Fund account 16201114.

References

Akahira, A., K.C.A. Alam, Y. Hamamoto, A. Akisawa, and T. Kashiwagi. 2004. Mass recovery adsorption refrigeration cycle-improving cooling capacity. *International Journal of Refrigeration* 27:225–34.

Alam, K.C.A., A. Akahira, Y. Hamamoto, A. Akisawa, and T. Kashiwagi. 2004. A four-bed mass recovery adsorption refrigeration cycle driven by low temperature waste/renewable heat source. *Renewable Energy* 29:1461–75.

Alam, K.C.A., B.B. Saha, and A. Akisawa. 2013. Adsorption cooling driven by solar collector: A case study for Tokyo solar data. *Applied Thermal Engineering* 50:1603–9.

Ambarita, H., and H. Kawai. 2016. Experimental study on solar-powered adsorption refrigeration cycle with activated alumina and activated carbon as adsorbent. *Case Studies in Thermal Engineering* 7:36–46.

Ammar, M.A.H., B. Benhaoua, and M. Balghouthi. 2015. Simulation of tubular adsorber for adsorption refrigeration system powered by solar energy in sub-Sahara region of Algeria. *Energy Conversion and Management* 106:31–40.

Anyanwu, E.E. 2004. Review of solid adsorption solar refrigeration II: An overview of the principles and theory. *Energy Conversion and Management* 45:1279–95.

Chan, K.C., C.Y. Tso, C.Y.H. Chao, and C.L. Wu. 2015. Experiment verified simulation study of the operating sequences on the performance of adsorption cooling system. *Building Simulation, Tsinghua University Press* 8:255–69.

Chan, K.C., C.Y.H. Chao, G.N. Sze-To, and K.S. Hui. 2012. Performance predictions for a new zeolite 13X/CaCl2 composite adsorbent for adsorption cooling systems. *International Journal of Heat and Mass Transfer* 55:3214–24.

EMSD. 2013. Hong Kong energy end-use data. *Electrical & Mechanical Services Department HKSAR*. http://www.emsd.gov.hk

Hassan, H.Z., A.A. Mohamad, and H.A. Al-Ansary. 2012. Development of a continuously operating solar-driven adsorption cooling system: Thermodynamic analysis and parametric study. *Applied Thermal Engineering* 48:332–41.

Hassan, H.Z., A.A. Mohamad, and R. Bennacer. 2011. Simulation of an adsorption solar cooling system. *Energy* 36:530–7.

Ji, X., X.B. Song, M. Li, J.X. Liu, and Y.F. Wang. 2015. Performance investigation of a solar hot water driven adsorption ice-making system. *Energy Conversion and Management* 106:759–65.

Khan, M.Z.I., B.B. Saha, K.C.A. Alam, A. Akisawa, and T. Kashiwagi. 2007. Study on solar/waste heat driven multi-bed adsorption chiller with mass recovery. *Renewable Energy* 32:365–81.

Koronaki, I.P., E.G. Papoutsis, and V.D. Papaefthimiou. 2016. Thermodynamic modeling and exergy analysis of a solar adsorption cooling system with cooling tower in Mediterranean conditions. *Applied Thermal Engineering* 99:1027–38.

Li, T.X., R.Z. Wang, J.K. Kiplagat, L.W. Wang, and R.G. Oliveira. 2009. A conceptual design and performance analysis of a triple-effect solid-gas thermochemical sorption refrigeration system with internal heat recovery. *Chemical Engineering Science* 64: 3376–84.

Loh, W.S., A.B. Ismail, B. Xi, K.C. Ng, and W.G. Chun. 2012. Adsorption isotherms and isosteric enthalpy of adsorption for assorted refrigerants on activated carbons. *Journal of Chemical and Engineering Data* 57:2766–73.

Miyazaki, T., A. Akisawa, B.B. Saha. 2010. The performance analysis of a novel dual evaporator type three-bed adsorption chiller. *International Journal of Refrigeration* 33:276–85.

Nidal, H., A. Hamdeh, and M.A. Al-Muhtaseb. 2010. Optimization of solar adsorption refrigeration system using experimental and statistical techniques. *Energy Conversion and Management* 51:1610–5.

Qasem, N.A.A., and M.A.I. El-Shaarawi. 2015. Thermal analysis and modeling study of an activated carbon solar adsorption icemaker: Dhahran case study. *Energy Conversion and Management* 100: 310–23.

Qu, T.F., R.Z. Wang, and W. Wang. 2001. Study on heat and mass recovery in adsorption refrigeration cycles. *Applied Thermal Engineering* 21:439–52.

Saha, B.B., A. Akisawa, and T. Kashiwagi. 2001. Solar/waste heat driven two-stage adsorption chiller: The prototype. *Renewable Energy* 23:93–101.

Saha, B.B., I.I. El-Sharkawy, A. Chakraborty, S. Koyama, N.D. Banker, P. Dutta, M. Prasad, and K. Srinivasan. 2006. Evaluation of minimum desorption temperatures of thermal compressors in adsorption refrigeration cycles. *International Journal of Refrigeration* 29:1175–81.

Sapienza, A., S. Santamaria, A. Frazzic, and A. Freni. 2011. Influence of the management strategy and operating conditions on the performance of an adsorption chiller. *Energy* 36:5532–8.

Solmus, I., B. Kaftanoglu, C. Yamali, and D. Baker. 2011. Experimental investigation of a natural zeolite-water adsorption cooling unit. *Applied Energy* 88:4206–13.

Thu, K., A. Chakraborty, B.B. Saha, and K.C. Ng. 2013. Thermophysical properties of silica gel for adsorption desalination cycle. *Applied Thermal Engineering* 50:1596–602.

Tso, C.Y., and C.Y.H. Chao. 2012. Activated carbon, silica-gel and calcium chloride composite adsorbents for energy efficient solar adsorption cooling and dehumidification systems. *International Journal of Refrigeration* 35:1626–38.

Tso, C.Y., C.Y.H. Chao, and S.C. Fu. 2012. Performance analysis of a waste heat driven activated carbon based composite adsorbent—Water adsorption chiller using simulation model. *International Journal of Heat and Mass Transfer* 55:7596–610.

Tso, C.Y., K.C. Chan, C.Y.H. Chao, and C.L. Wu. 2015. Experimental performance analysis on an adsorption cooling system using zeolite13X/$CaCl_2$ adsorbent with various operation sequences. *International Journal of Heat and Mass Transfer* 85:343–55.

Tso, C.Y., S.C. Fu, and C.Y.H. Chao. 2014. Modeling a solar-powered double bed novel composite adsorbent (silica activated carbon/$CaCl_2$) adsorption chiller using. *Building Simulation* 7:185–96.

Ullah, K.R., R. Saiur, H.W. Ping, R.K. Akikur, and N.H. Shuvo. 2013. A review of solar thermal refrigeration and cooling methods. *Sustainable Energy Review* 24:499–513.

Wang, D.C., Y.H. Li, D. Li, Y.Z. Xia, and J.P. Zhang. 2010. A review on adsorption refrigeration technology and adsorption deterioration in physical adsorption systems. *Renewable and Sustainable Energy Reviews* 14:344–53.

Wang, Q., X. Gao, J.Y. Xu, A.S. Maiga, and G.M. Chen. 2012. Experimental investigation on a fluidized-bed adsorber/desorber for the adsorption refrigeration system. *International Journal of Refrigeration* 35:694–700.

Wang, R.Z. 2001. Adsorption refrigeration research in Shanghai Jiao Tong University. *Renewable and Sustainable Energy Reviews* 5: 1–37.

Zhu, L.Q., C.L. Wu, T.C. Chan, K.C. Chan, G.N. Sze-To, and C.Y.H. Chao. 2013. Development of a new multi-chamber double-layer adsorber in energy efficient solar adsorption cooling systems. *Proceedings of the APEC Conference on Low Carbon Town and Physical Energy Storage*, Changsha, China, May 25–26, E02-15: 125–30.